Modeling of West Florida Shelf Circulation for Spring 1999

Ruoying He and Robert H. Weisberg
College of Marine Science, University of South Florida
140 7th Ave. South, St. Petersburg, Florida, 33701

Abstract

Mid-latitude continental shelves undergo a spring transition as the net surface heat flux changes from cooling to warming. Using *in-situ* data and a numerical circulation model we investigate the circulation and temperature budget on the West Florida Continental Shelf (WFS) for the spring transition of 1999. The model is a regional adaptation of the primitive equation, Princeton Ocean Model forced by NCEP re-analysis wind and heat flux fields and by river inflows. Based on agreements between the modeled and observed fields we use the model to draw inferences on how the surface momentum and heat fluxes affect the seasonal and synoptic scale variability. We account for a strong southeastward current at mid-shelf by the baroclinic response to combined wind and buoyancy forcing, and we show how this local forcing leads to annually occurring cold and low salinity tongues. Through term-by-term analyses of the temperature budget we describe the WFS temperature evolution in spring. Heat flux largely controls the seasonal transition, whereas ocean circulation largely controls the synoptic scale variability. Rivers contribute to the local hydrography and are important ecologically. Along with upwelling, river inflows facilitate frontal aggregation of nutrients and the spring formation of a high concentration chlorophyll plume near the shelf break (the so-called 'Green River'), coinciding with the cold, low salinity tongues. These features originate by local, shelf-wide forcing; the Loop Current is not an essential ingredient for spring transition of 1999.

1. Introduction

Located at the eastern edge of the Gulf of Mexico, the West Florida Continental Shelf (WFS) is one of the broadest continental shelves in North America. Between its southern and northern ends, bounded by the Florida Keys and the Florida Big Bend, respectively, the WFS isobaths vary smoothly, and they generally parallel the coastline (Fig 1). This geometry changes along the Florida

Panhandle in the north where the coastline undergoes a right angle bend, and the shelf width decreases to a minimum at the DeSoto Canyon.

Long-term observations (*Weisberg et al.*, 1996) show that the WFS circulation, forced by tides, winds, buoyancy, and possible interactions with the Gulf of Mexico Loop Current, varies on time scales from semi-diurnal to inter-annual. Monthly mean currents at mid-shelf suggest a seasonal cycle with along-shore flows either to the southeast in spring, or to the northwest in late summer to early autumn. *Weisberg et al.* (1996) hypothesized that these seasonal currents are of a baroclinic nature based on an observed thermal wind shear and the seasonal reversal of the across-shelf density gradient. As a consequence of the spring transition in surface heat flux from cooling to warming, they argued that spatial differences in heating (from the coast to offshore by increasing depth and from the south to north by solar declination) form a mid-shelf cold tongue and a seasonally maximum across-shelf density gradient that supports a southeastward current. Here we examine this locally forced, seasonal circulation hypothesis by focusing on the spring transition for 1999, a year when the Loop Current, as evidenced in relatively flat isopycnal topography at the shelf break, did not have a strong direct influence the WFS. Our objective is to describe the circulation and temperature budget for spring 1999 with respect to the shelf-wide winds, surface heat fluxes, and river inflows.

The observational record [e.g. *Niiler,* 1976; *Mitchum and Sturges*, 1982; *Cragg et al.*, 1983; *Marmorino*, 1983] shows that the WFS circulation and sea level variations are highly correlated with the synoptic scale wind stress variations. The passage of cold fronts also affects the local temperature balance (e.g., *Price,* 1976). Along with these local synoptic scale variations are baroclinic effects that originate with the Loop Current at the shelf break [e.g., *Paluszkiewicz et al.*, 1983]. What remains unclear is the relative importance of the momentum and buoyancy that are input either locally, or at the shelf break.

Such questions are of multi-disciplinary interest since, despite its oligotrophic description, the WFS supports highly productive ecosystems. These include episodic toxic dinoflagellate blooms (red tides) near the coast, a seasonal chlorophyll plume (so called 'green river') near the shelf break (*Gilbes et al.*, 1996), and important commercial and recreational fisheries throughout the WFS. Parallel programs of *in situ* measurements and numerical model experiments are presently in place for an improved understanding of the circulation and how it affects seasonally varying water properties and influences organism growth and distribution.

This paper focuses on local wind and buoyancy forcing during the spring transition of 1999, independent of the Loop Current. We use the primitive equation, Princeton Ocean Model (POM) described by Blumberg and Mellor (1987) forced by National Center for Environmental Predication (NCEP) re-analysis winds and net surface heat flux and by river inflows. The only role of the adjacent Gulf of Mexico is to set the vertical distribution of temperature and salinity for initializing the model density field. Once begun, the integration proceeds solely on the basis of local forcing. By running twin experiments, one

with heat flux and the other without, we explore the relative importance of wind and buoyancy in affecting the seasonal and synoptic scale variability.

Section 2 describes the model and forcing fields. Section 3 compares model results with *in-situ* observations. Based upon these comparisons the model is used in section 4 to describe the seasonal mean circulation of the WFS for spring 1999 and the evolution of the corresponding temperature and salinity fields. Section 5 presents a term-by-term analysis of the three-dimensional temperature budget. The results are summarized and discussed in section 6.

2. Model and Forcing fields

2.1. Model

We use the POM for the following reasons. First, it has an embedded turbulence closure sub-model (*Mellor and Yamada,* 1982) for parameterizing vertical turbulence mixing. Second, it employs a sigma coordinate in the vertical which, with the turbulence closure sub-model, is well suited to study the nonlinear dynamics over a shallow, gently sloping continental shelf. Third, its orthogonal curvilinear coordinates in the horizontal are convenient for resolving the near-shore regions.

The model domain (Fig 1) extends from the Florida Keys in the southeast to west of the Mississippi River in the northwest, and it has one open boundary arcing between these two locations for which a radiation boundary condition (*Orlanski,* 1976) is used. The model domain includes the major rivers that impact the WSF and the Desoto Canyon region where the shelf is narrowest, and its orthogonal curvilinear grid has horizontal resolution that varies from less than 2km near the coast to 6 km near the open boundary. Vertically, the sigma coordinate has 21 layers with higher resolution near the surface and bottom to better resolve the frictional boundary dynamics. In total, the model has 121×81×21 grid points. Horizontal diffusivities are parameterized using the *Smagorinsky* (1963) formulation with a dimensionless coefficient of 0.2. Bottom stress, τ_b, is calculated by a quadratic law with variable drag coefficient having a minimum value of 0.0025. A mode splitting technique is used for computational efficiency (*Blumberg and Mellor,* 1987). Here we use external and internal time steps of 12 seconds and 720 seconds, respectively.

The model is initialized at rest with horizontally uniform stratification. Stratification above 200 m is based on temperature and salinity observations taken during a March 1999 trans-shelf hydrographic survey [from the Ecology of Harmful Algal Blooms (ECOHAB) Program]. Stratification below 200 m is based on Levitus climatology. From this initial zero-baroclinicity state, the model spins up rapidly, generating baroclinicity in balance with the wind and buoyancy forcing. An alternative is to begin with a baroclinic field and allow the model currents to come into balance diagnostically with this field before proceeding with the spring simulation. The hydrographic data are not sufficient for this, however, and spurious currents due to incorrect density would corrupt the experiment.

Consistent with our objective of determining the WFS responses to local, shelf-wide forcing only, our initial baroclinicity-free state is a sensible choice.

Tidal forcing is excluded in the present application since we are not considering high frequency variability. It is recognized that tidal mixing can affect the synoptic and seasonal scales when the tidal currents are large, but here the tidal currents are only a few cm s^{-1} (*He and Weisberg*, 2001).

2.2 Atmospheric forcing

Different from previous WFS model studies that considered wind forcing only, here we include both wind and thermohaline forcing. The wind and heat flux fields are derived from the NCEP daily re-analysis product for the period February 28 to June 1, 1999. These values, with a grid resolution of 2.5°×2.5°, are interpolated onto the model grid. The NCEP winds agree well with *in-situ* buoy winds for the spring 1999 season. Unlike the winds, however, coarse resolution renders the NCEP heat flux unrealistic because of smaller scale WFS temperature structures. We correct for this using a relaxation method (*e.g., Ezer and Mellor*, 1992; *Chu et al.*, 1999). Thus, the surface fluxes forcing are given by

$$K_H \frac{\partial \theta}{\partial z} = \left(\frac{Q_H}{\rho C_P} \right) + C(\theta_{obs} - \theta)$$
$$K_H \frac{\partial S}{\partial z} = 0 \qquad (1)$$

where θ and S are temperature and salinity, respectively. Q_H is the net heat flux, θ_{obs} is an interpolation of the monthly-mean satellite observed sea surface temperature, and C_p is the specific heat. The salinity flux in this study is set to be zero. The relaxation coefficient, C, or the reciprocal of the restoring time per unit area, is set at 1m/day. Such relaxation prevents deviations from observed monthly-mean SST in an attempt to force realistic baroclinic flow structures. These structures are facilitated by turbulent mixing through the turbulent eddy viscosity and diffusivity K_M and K_H computed with the *Mellor and Yamada* (1982) 2.5 level turbulence closure sub-model.

2.3 Lateral boundary forcing.

Gulf of Mexico Loop Current forcing is excluded in this study for two reasons. First, previous observations and model studies concluded that persistent forcing of the middle and inner-shelf by the Loop Current is minimal (*Marmorino*, 1983). Second, modeling the effects on the WFS of an aperiodically varying Loop Current and its associated eddies (e.g., *Sturges and Leben*, 2000) remains a great challenge (*Marmorino*, 1983; *Cooper*, 1987), presupposing that the Loop Current itself is being described properly. To better assess the role of the Loop Current as a WFS boundary condition it will be necessary to nest a regional model with a larger Gulf of Mexico/Caribbean/Atlantic Ocean model. This is beyond the scope of the present paper that focuses on local, shelf-wide forcing only. We find, however, that local forcing is capable of driving much of the observed synoptic and seasonal scale variability.

Seven major rivers are introduced into the model domain for land derived buoyancy forcing. These are the Mississippi, Mobile, Apalachicola, Suwannee, Hillsborough, Peace and Shark rivers. We use the technique of *Kourafalou et al.* (1996)[also see *Pullen* 2000], whereby interpolated monthly mean mass flux data for these rivers are input to the top sigma level at the grid cells closest to the rivers' locations. The salinity of rivers are set as zero and the temperature are temporally linear interpolated between the climatological March mean and May mean water temperature.

We define the spring season here as March 1 to May 31, and we focus on this period for 1999. As an initial value problem we begin from a state of rest on February 28. With no initial baroclinicity, the spin-up phase proceeds rapidly over the course of a few pendulum days, consistent with the barotropic response arguments for a gently sloping shelf of *Clarke and Brink* (1985). Under the conditions of surface cooling that occur prior to the spring warming transition in mid-March, convective mixing very efficiently adjusts the initial density field on the shallow shelf. In other words, the "memory" of initial density field for this spring transition experiment is short, and sensitivity experiments that we performed using longer spin-up times showed very little difference from the present model results.

3. Model and Data Comparisons

3.1 Sea level

Since the model is forced without tides, all of the model and data comparisons are shown after low-pass filtering to exclude tidal and inertial period oscillations. Sea surface height comparisons are given in Fig. 2 at four different NOAA tide-gauge stations from Pensacola in the northwest to Naples in the southeast. Agreement is good at all of these with squared correlation coefficients exceeding 0.80. We conclude that coastal sea level for this three-month period responds primarily to local, shelf-wide forcing.

3.2 Currents

Comparisons are made between the modeled and observed velocity vector time series at the 50m, 30m, 25m, 20m, and 10m isobaths (moorings CM2, EC3, NA2, EC4, EC5, and EC6 in Fig. 1). The observations are from Acoustic Doppler Current Profilers (ADCP), and for each location we show comparisons at three different depths: near-surface, mid-water column, and near-bottom. These comparisons are quantified by a complex correlation analysis (*e.g., Kundu* 1976). Defining the modeled and observed velocity vectors in the Argand plane as $w_1 = u_1 + iv_1$ and $w_2 = u_2 + iv_2$, respectively, the complex squared correlation coefficient is

$$\rho^2(w_1, w_2) = \frac{\overline{[w_1^*(t)w_2(t)]}^2}{\overline{[w_1^*(t)w_1(t)]}\ \overline{w_2^*(t)w_2(t)]}} \qquad (2)$$

where the overbar denotes a time average. The complex correlation has an amplitude and a phase, the amplitude being the correlation coefficient and the phase being the angle (measured counterclockwise) between the modeled and the observed currents. As an example of these comparisons, Fig.3 shows the modeled and observed vector time series at 10m location (EC5). Like sea level, the modeled and observed currents also compare well as measured by the two sets of numbers provided with each plot. The left-hand sets are the seasonal mean east and north velocity components. The right-hand sets are the squared correlation coefficient, phase angle, and regression coefficient. At all stations and depths the squared correlation coefficients range between 0.62-0.82, and the orientations agree to within –10 to +20 degrees. More importantly, as seen directly from the time series, the model gets the sense of the velocity rotation correct in both the surface and bottom Ekman layers. A deficiency in the modeled currents, however, lies in the amplitudes. The regression coefficients show that the model underestimates the observed velocity fluctuations by between 20 to 50 percent.

Notwithstanding the amplitude disparity, the model reproduces the patterns of current variability reasonably well. The systematic underestimate of the currents may be the result of the low-resolution NCEP forcing fields, and hence too much smoothing when interpolating these fields onto the model grid. Model performance also degrades between the shallowest and deepest comparison sites, i.e., the 10 m isobath currents agree better than the 50 m isobath currents. This is expected based on the frictional scale of the inner-shelf response to wind forcing (*e.g., Weisberg et al.*, 2001). The 50 m isobath is at the outer half of the inner-shelf so we anticipate a decreased correlation there.

The modeled and observed velocity comparisons are summarized in Fig. 4 where we show the mid-depth seasonal mean vectors and hodograph ellipses at all of the mooring locations. The mean vectors compare reasonably well, and while the ellipse semi-major axes are off by between 20-50%, the orientations and eccentricities tend to agree. On the basis of these agreements we now use the model to discuss the WFS circulation in spring 1999.

4. Mean Circulation

4.1 Flow fields

The seasonal mean circulation, obtained by averaging the model flow fields from March 1 to May 31, is presented in Fig 5a. The depth-averaged fields show the general nature of the 1999 spring season currents. A jet exists with axis situated between the mid-shelf and the shelf break. This jet originates along the northern coast east of the Mississippi River, and it flows along the relatively narrow Florida Panhandle shelf as a closely confined coastal feature. The coastal jet bifurcates at Cape San Blas into a mid-shelf part that heads along-isobath toward the southeast and a coastal part that hugs the Big Bend coastline. The mid-shelf part is consistent with the spring season southeastward current described by *Weisberg et al.* (1996). This mid-shelf current again bifurcates upon approaching the Florida Keys with a portion turning toward Florida Bay and

another portion turning farther offshore. We also note that the currents within the Big Bend and those that flow southward near-shore between Cedar Key and Sarasota are much weaker than the currents at mid-shelf. As will be shown in the next section, this is a consequence of a surface heat flux-induced cyclonic circulation that adds destructively (constructively) to the wind driven flow near-shore (offshore).

4.2 Temperature and salinity fields

The modeled surface temperature and salinity fields sampled at the end of the model run on May 31 are presented in Fig 5 b, c. Since the initial model temperature and salinity fields are horizontally uniform, this figure shows the combined effects of the momentum and buoyancy fluxes in changing the surface temperature and salinity. The two principal features are the mid-shelf cold tongue that extends southeastward from Cape San Blas and the low salinity tongue that also extends southeastward, but displaced seaward of the cold tongue. Both of these features occur annually on the WFS. The cold tongue is imposed to some extent through the surface heat flux relaxation, whereas the low salinity tongue is a fully prognostic result of the model.

The low salinity tongue derives as a river plume, accumulating fresh water primarily from the Mississippi River with additions from the Mobile and Apalachicola Rivers. Modulated inter-annually, the low salinity tongue extends southward each year, and in some years (1993, for instance – see *Dowgiallo*, 1994) it can be traced around the Florida peninsular to the Carolinas. Using Coastal Zone Color Scanner data between 1979 and 1986, *Gilbes et al.* (1996) reported a spring chlorophyll plume at mid-shelf (termed the 'Green River') that also extends southeast from Cape San Blas. Their explanations for the plume included: *i.* nutrient fluxes from the Apalachicola River; *ii.* nutrient fluxes from the Mississippi and Mobile Rivers; *iii.* seasonal changes in steric height between the shelf and deeper Gulf of Mexico; and *iv.* circulation of water from the Loop Current. Our results help to clarify these speculations. Consistent with *Weisberg et al.* (1996) the 'Green River' is associated with both the cold tongue and the low salinity tongue. The low salinity tongue, at least in 1999, appears to originate at the Mississippi, Mobile and Apalachicola Rivers. It is advected eastward, on average, by the spring coastal jet and then southeastward where the jet bifurcates at Cape San Blas. This bifurcation, in part, is related baroclinically to the cold tongue; hence the offset between the low salinity and cold tongues. Since the Loop Current is not included in our model, and since it did not extend to the northeast Gulf of Mexico in spring 1999, we can rule out the Loop Current as a primary conveyance of these salinity and temperature features for this time period.

4.3. Twin experiments

To understand the importance of surface heat flux on the seasonal circulation, it is instructive to see how the baroclinic contribution evolves. This is shown in Fig. 6 for the March, April, and May monthly mean, depth-averaged

flows in addition to the depth averaged seasonal mean. March shows an anticyclonic circulation with southeastward flow near-shore. During April, once the effects of positive heat flux set in, we see the formation of the mid-shelf jet and a cessation or reversal of the near-shore flow. This further develops into a strong mid-shelf/shelf-break current in May as the cyclonic baroclinic flow becomes fully developed. Baroclinicity explains how this happens. During early spring, surface heat flux is out of the ocean, the cooling effect produces offshore thermal gradients, causing a southeastward baroclinic current. This current superimposes on the wind-driven part, resulting in a stronger coastal jet. In later spring, the effect of surface heat flux changes from cooling to warming and heats up the shallow water quickly. With wind and heat flux forcing, a dynamical feedback occurs with the cold tongue causing a cyclonic baroclinic circulation that adds constructively (destructively) with the wind forced circulation at mid-shelf (near-shore).

Realizing the roles of surface heat fluxes in the formation of circulation and temperature features, we ran a model twin experiment forced by NCEP winds only. Temperature cross-sections at various positions along the WFS provide further information on the cold tongue evolution. These are shown for wind and heat flux forcing and for wind forcing only on March 15, and April 15 in Fig 7a and 7b, respectively, at four transects offshore of DeSoto Canyon (I), Cape San Blas (II), the Big Bend (III), and Sarasota (IV). Since the heat flux is initially out of the ocean the March 15 transects, with or without heat flux, are similar at depth. They differ on the inner shelf where surface cooling, coupled with efficient convective mixing, produces typical wintertime horizontal stratification. By April 15, with a reversal in the sign of the heat flux, the two cases depart almost everywhere. For the case with surface heat flux, the shelf water is stratified and the modeled temperature agrees well with observed ECOHAB Program hydrography. For the case without the surface heat flux, the shelf water is still well mixed and cold. The cold tongue on the middle shelf and the baroclinic feedback forced by both wind and heat flux as mentioned above do not exist.

5. Temperature Budget

5.1 The temperature equation

To analyze the temperature budget, the temperature equation is recast from its modeled flux divergence, *sigma level* form to an advective, *z-level* form. Thus, we diagnose

$$\underset{a}{\frac{\partial T}{\partial t}} = \underset{b}{-u\frac{\partial T}{\partial x}} \underset{c}{-v\frac{\partial T}{\partial y}} \underset{d}{-w\frac{\partial T}{\partial z}} \underset{vf}{+\frac{\partial}{\partial z}\left(K_H \frac{\partial T}{\partial z}\right)} \underset{hf_x}{+\frac{\partial}{\partial x}\left(A_H \frac{\partial T}{\partial x}\right)} \underset{hf_y}{+\frac{\partial}{\partial y}\left(A_H \frac{\partial T}{\partial y}\right)} \qquad (3)$$

which equates the local rate of change of temperature *(a)* to a combination of the flow field advective rate of change *(b+c+d)*, and the rates of change by vertical diffusion *(vf)*, and horizontal diffusion *(hf_x+hf_y)*. The temperature balance is

explored using time series of vertical averages and vertical profiles at four different locations.

The four analysis locations A, B, C and D (see Fig. 1) are chosen with respect to the cold tongue and the upwelling region north of the Florida Keys. Point A is on the 50 m isobath at the seaward side of the Big Bend shelf subsurface cold dome. Point B is on the 40 m isobath west of Tampa Bay where the cold tongue begins to taper off. Point C is on the 15 m isobath offshore of Sarasota on the inshore side of the cold tongue. Point D is north of the Florida Keys. A term-by-term analysis of Equation (3) quantifies the contributions by each physical process in changing the temperature.

5.2 Depth-averaged balances.

A depth-averaged temperature equation is obtained by vertically integrating equation (3). Since horizontal temperature diffusion is generally at least an order of magnitude less than the other terms, the depth-averaged diffusion term is essentially the depth-averaged vertical diffusion, $Q/(\rho C_P H)$, where Q is the net surface heat flux, ρ and C_P are the seawater density and specific heat, and H is the water depth. The temperature variations depend on both ocean advection and diffusion. With a two-dimensional model, *Morey* (1999) proposed that temperature, in a depth-averaged sense, could be well represented without advection, i.e.,

$$\frac{dT}{dt} = \frac{\partial T}{\partial t} = \frac{Q(t)}{\rho c_P H} \tag{4}$$

The validity of this assertion for various locations on the WFS can be evaluated by a fully three-dimensional analysis.

As an example, time series of the depth-averaged ocean advection and diffusion terms and their sum for location C (15 m isobath) are shown in Fig. 8a. It is seen that the seasonal change (as given by the three-month mean values) is primarily by surface heat flux, whereas the synoptic variability (as given by the standard deviations) is primarily by ocean advection. Of the total change in vertically averaged temperature (4.76^{0}C), the contributions by ocean advection and surface heat flux are cooling of -1.24^{0}C and a warming of 6.00^{0}C, respectively. Similar diagnoses are made at locations A, B and D. It is found that the effect of ocean circulation on the seasonal mean temperature change and the magnitude of the controlling ocean circulation effect on the synoptic scale variability decrease with increasing water depth.

5.3 Vertical profiles of the term-by-term balances

The temperature budget three-dimensionality is further explored through time series of the depth profiles of the individual terms that compose the temperature balance at these four stations. Fig. 8b shows the temperature budget at station C. The left panels of the figure show the horizontal and vertical components of the ocean advection and their sum, and the right panels show the diffusion, the diffusion plus the advection (which is nearly exactly equal to the

local rate of change of temperature), and the temperature. With the exception of the initial portion of the record when the surface heat flux is out of the ocean and convective mixing is evident, the impact of the surface heat flux is primarily warming. Through turbulent mixing brought about by the ocean circulation dynamics, the surface heat flux effect penetrates downward to make its contribution to the depth-averaged spring transition. Along with its role in turbulence mixing, the direct role of warming and cooling by the ocean dynamics through advection on the synoptic scale variability is seen in both horizontal and vertical directions. Omission of advection in any coordinate direction would compromise the model's ability to describe the temperature evolution.

6. Summary

Mid-latitude continental shelves undergo a spring transition as the net surface heat flux changes from cooling to warming. Using *in-situ* data and a numerical circulation model we investigate the circulation and temperature budget on the WFS, including the northeast Gulf of Mexico shelf from the Mississippi River to the Florida Keys, for the spring transition of 1999. The data consist of sea level from coastal stations, velocity profiles from instruments moored across the shelf between the 50 m and 10 m isobaths, and hydrography from ship surveys. The model is a regional adaptation of the primitive equation, POM forced by NCEP re-analysis wind stress and heat flux fields and by river inflows. Based on agreements between the modeled and observed fields we use the model to draw inferences on how the surface momentum and heat fluxes affect the seasonal and synoptic scale variability.

Spring season features of the WFS include a mid-shelf southeastward current, cold and low salinity tongues, and a high chlorophyll plume. We account for the southeastward current in 1999 by the combined responses to local, shelf-wide wind and buoyancy forcing. Wind stress drives a circulation that tends to be strongest near-shore. Heat flux provides a cyclonic contribution that adds constructively (destructively) at mid-shelf (near-shore), thus forming the observed mid-shelf jet. This heat flux-induced baroclinic circulation is related to the spring season cold tongue. By advecting Mississippi (and other) River water, the circulation forms the low salinity tongue that is displaced seaward of the cold tongue. Convergence of nutrients and associated phytoplankton growth then accounts for the high chlorophyll concentrations ('Green River') that are co-located with these surface features. These findings support the hypothesis advanced by *Weisberg et al.* (1996) on the origin of the southeastward current and cold tongue through differential heating from the coast to offshore (by shoaling topography) and from south to north (by solar declination). Since we arrive at these features with a model experiment that explicitly omits the Gulf of Mexico Loop Current we argue that the Loop Current is not an essential element of these spring transition features for this time period.

Through term-by-term analyses of the temperature budget we describe the evolution of the WFS temperature in spring. Surface heat flux largely controls

the seasonal transition, whereas ocean circulation largely controls the synoptic scale variability. Varying in both time and space, the temperature evolution on the WFS depends on fully three-dimensional thermodynamics.

Acknowledgments

This work was supported by grants from the Office of Naval Research, grant # N00014-98-1-0158 and the National Oceanic and Atmospheric Administration, grant #NA76RG0463. We also benefited from an evolving program with previous support from the United States Geological Survey and the Minerals Management Service and the state of Florida Coastal Ocean Monitoring and Prediction System. Ocean Circulation Group staff (Messrs. R. Cole, J. Donovan, C. Merz, and P. Smith) contributed to the fieldwork and analyses. We thank F. Muller-Karger for providing assistance with the monthly mean SST fields. NCEP re-analysis data provided by NOAA-CIRES Climate Diagnostics Center, Boulder, CO was obtained from their web site at http://www.cdc.noaa.gov/

References

Blumberg, A. F., and G. L. Mellor. (1987), A description of a three-dimensional coastal ocean circulation model, *Three-Dimensional Coastal Ocean Models*, Vol. 4, N. Heaps (ed.), 208-233, AGU, Washington, D. C.

Chu, P. Edmons, N. and Fan, C. (1999), Dynamical mechanisms for the south China sea seasonal circulation and thermohaline variabilities. *J. Phys. Oceanogr.*, 29, 2971-2989

Clarke, A. J., and K. H. Brink. (1985), The response of stratified, frictional flow of shelf and slope waters to fluctuating large-scale, low-frequency wind forcing, *J. Phys. Oceanogr.*,15, 439-453

Cooper, C. (1987), A numerical modeling study of low-frequency circulation on the west Florida shelf, *Coastal Engineering*, 11, 29-56

Cragg, J., G. Mitchum, and W. Sturges. (1983), Wind-induced sea-surface slopes on the West Florida shelf, *J. Phys. Oceanogr.*, 13, 2201-2212

Dowgiallo, M.J., ed. (1994), Coastal oceanographic effects of the summer 1993 Mississippi River flooding, Special NOAA Report, 77pp.

Ezer, T., and G. Mellor (1992), A numerical study of the variability and separation of the Gulf Stream, induced by surface atmospheric forcing and lateral boundary flows. *J. Phys. Oceanogr.* 22, 660-682

Gilbes, F., C. Thomas, J. J. Walsh, and F. E. Muller-Karger. (1996), An episodic chlorophyll plume on the West Florida Shelf, *Continental Shelf Research*, 16, 1201-1224

He, R., and R. H. Weisberg. (2001), Tides on the West Florida Shelf, *J. Phys. Oceanogr.* Submitted,

Kourafalou, V. H., L.-Y. Oey, J.D. Wang, and T.L. Lee. (1996), The fate of river discharge on the continental shelf. 1: Modeling the river plume and the inner shelf coastal current. *J.Geophys. Res.*, 101, 3415-3434

Kundu, P.K. (1976), An analysis of inertial oscillations observed near the Oregon coast. *J. Phys. Oceanogr.* 6, 879-893

Marmorino, G. O. (1983), Variability of current, temperature, and bottom pressure across the West Florida continental shelf, winter, 1981-1982, *J. Geophys. Res.*, 88, c7, 4439-4457

Mellor, G.L. and T. Yamada. (1982), Development of a turbulence closure model for geophysical fluid problems, *Rev. Geophys.*, 20, 851-875

Mitchum, T. G., and W. Sturges. (1982), Wind-driven currents on the West Florida shelf, *J. Phys. Oceanogr.*, 12, 1310-1317

Morey, S.L. (1999),. The spring transition of thermal stratification on a mid-latitude continental shelf. Ph.D. dissertation, Florida State University, 51, 1999

Niiler, P. P. (1976), Observations of low-frequency currents on the West Florida continental shelf, *Memoires Societe Royale des Sciences de Liege*, 6, X, 331-358

Orlanski, I. (1976), A simple boundary condition for unbounded hyperbolic flows, *J. Comput. Phys.*, 21, 251-269

Paluszkiewicz, T., L. Atkinson, E.S. Parmentier, and C.R. McClain. (1983), Observation of a Loop Current front eddy intrusion onto the West Florida Shelf, *J. Geophys. Res.*, 88, 9636-9651

Price, J. F. (1976), Several aspects of the response of shelf waters to a cold front passage, *Memories Societe Royale des Sciences de Liege*, 6, X, 201-208

Pullen, J.D. (2000), Modeling studies of the coastal circulation off northern California, *Ph.D. Dissertation*, Oregon State University

Smagorinsky, J. (1963), General circulation experiments with primitive equations. I. The basic experiment. *Mon. Weather. Rev.*, 91, 99-164

Sturges, W., and R. Leben. (2000), Frequency of ring separations from the loop current in the Gulf of Mexico: A revised estimate. *J. Phys. Oceanogr.*, 30, 1814-1819

Weisberg, R. H., B. D. Black, H. Yang. (1996), Seasonal modulation of the West Florida continental shelf circulation, *Geophys. Res. Lett.*, 23,2247-2250

Weisberg, R. H., Z. Li, F. Muller-Karger. (2001), West Florida shelf response to local wind forcing, April 1998. *J.Geophy. Res., J. Geophys. Res.,* 106 (C12) 31,239-31,262

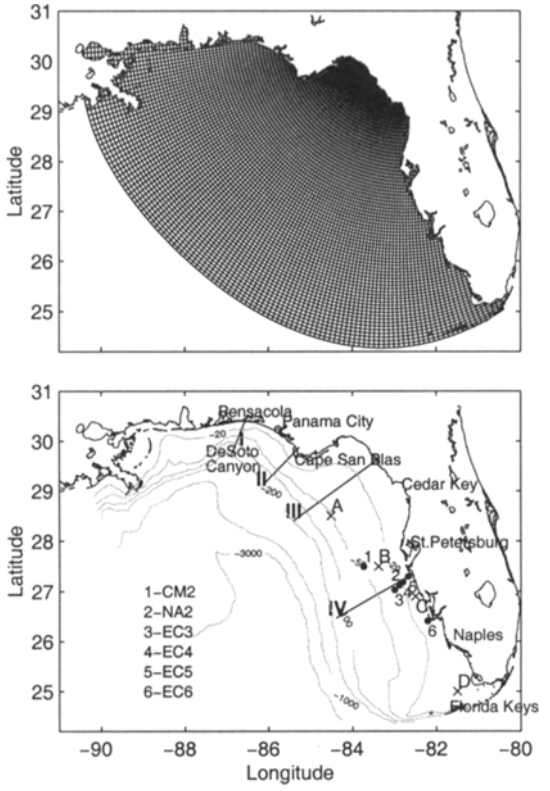

Figure 1 The regional model grid (upper panel) and bathymetry and station locations (lower panel). Sea level comparisons are with Florida tide gauges at Pensacola, Apalachicola, St. Petersburg, and Naples. Velocity comparisons are with acoustic Doppler current profiles from instruments moored at the 50m, 30m, 25m, 20m, and 10m isobaths (1-6). Temperature is described along transects I-IV, and the temperature budget is diagnosed at Stations A, B, C, and D.

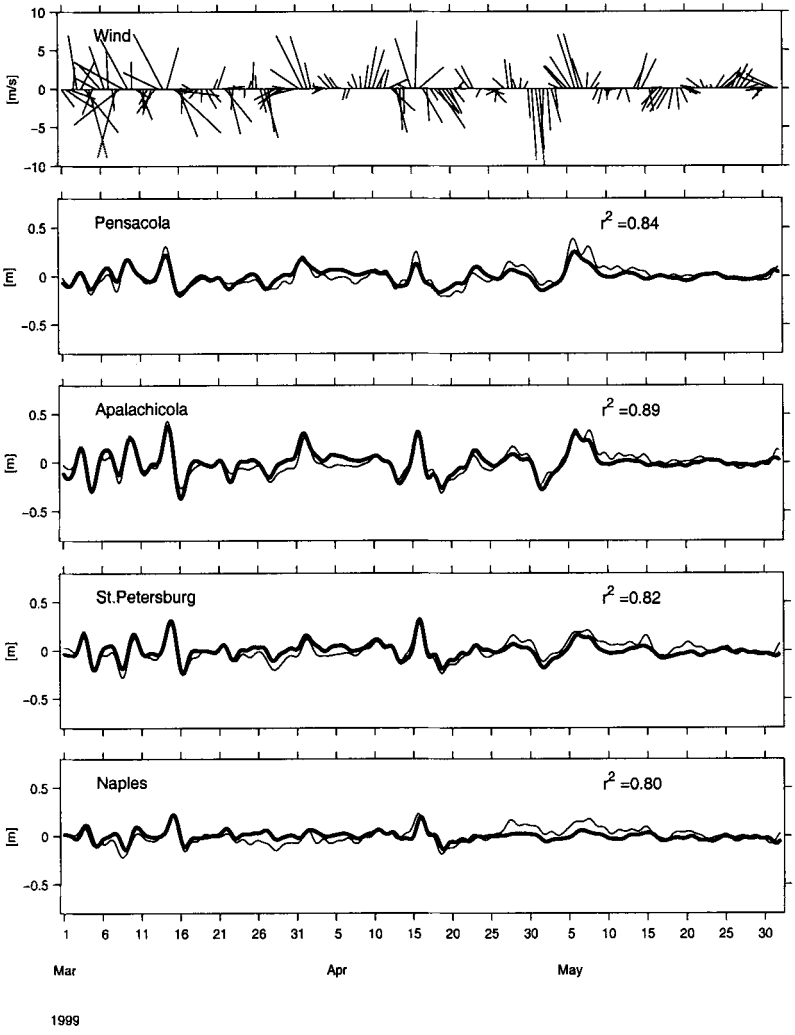

Figure 2 Comparisons between modeled (bold) and observed (thin) sea level at Pensacola, Apalachicola, St. Petersburg, and Naples as quantified by a squared correlation coefficient, along with the NCEP wind velocity sampled at station A.

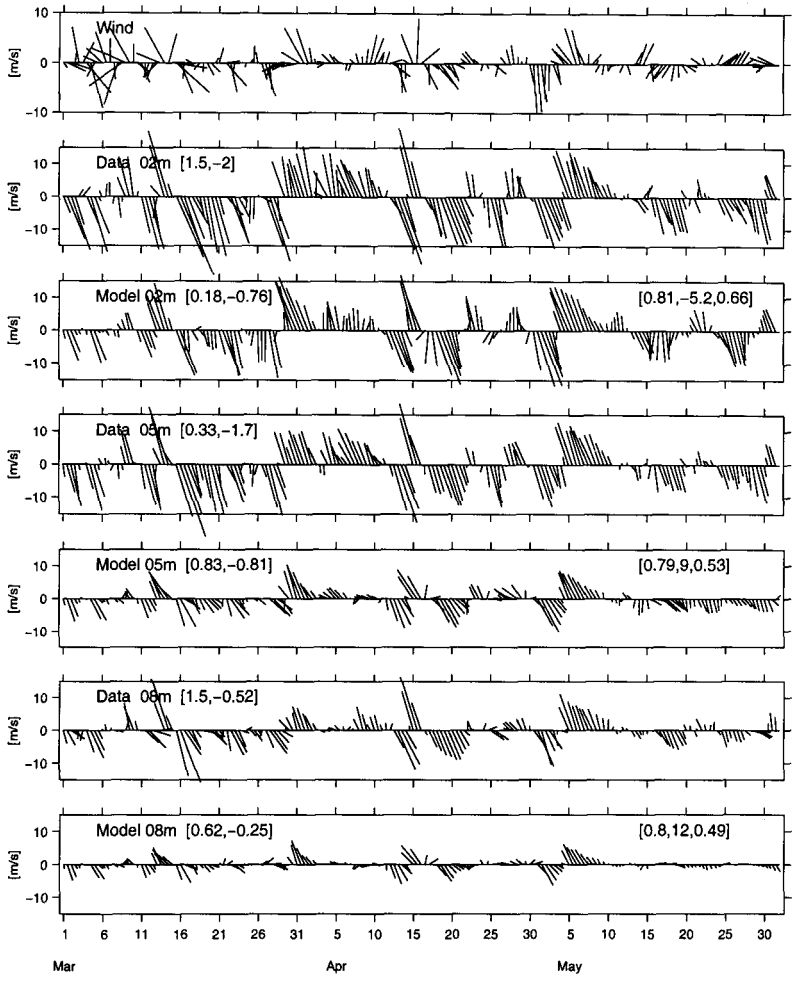

Figure 3 Comparisons between modeled and observed currents at the 10m isobath (mooring EC5) sampled at depths of 2m, 5m and 8m, along with the NCEP wind velocity sampled at station A. Each vector current time series is accompanied by its seasonal mean east and north velocity components (left hand couplet), and each model/data comparison is quantified by its squared complex correlation coefficient, phase angle (or angular deviation of the model vector from the data vector measured counterclockwise), and regression coefficient (right hand triplet).

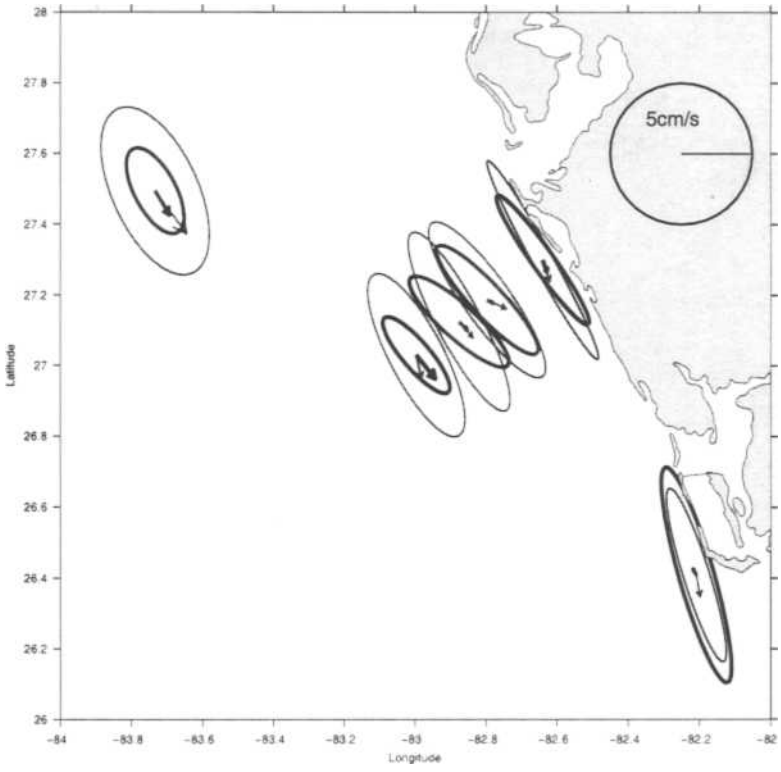

Figure 4 Comparisons between modeled (bold) and observed (thin) seasonal mean velocity vectors and hodograph ellipses at mid-depth for all six mooring locations on the WFS between the 50m and 10m isobaths.

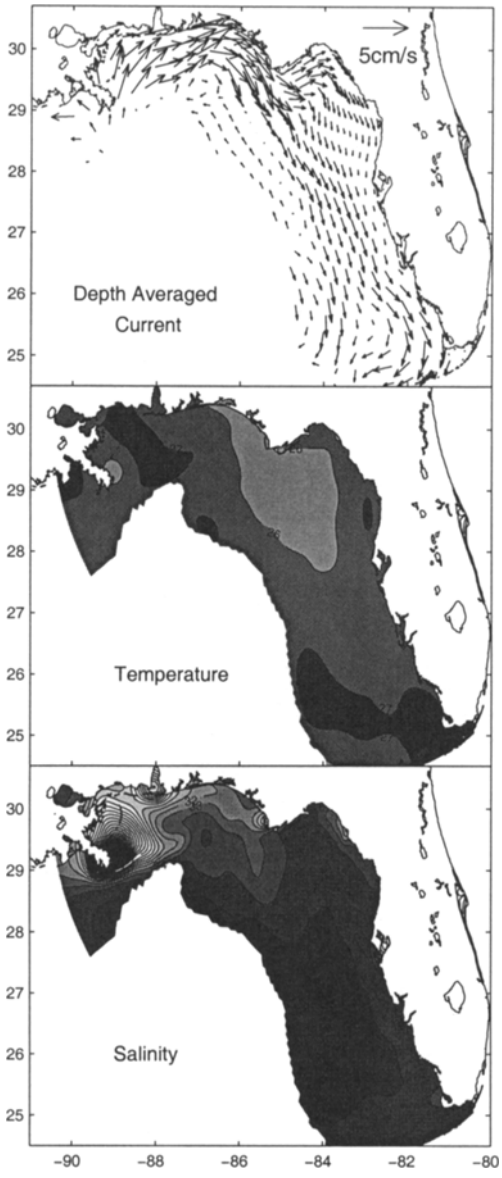

Figure 5 (a) Modeled seasonal mean depth-averaged current, (b) modeled sea surface temperature on May 31 and (c) modeled sea surface salinity on May 31.

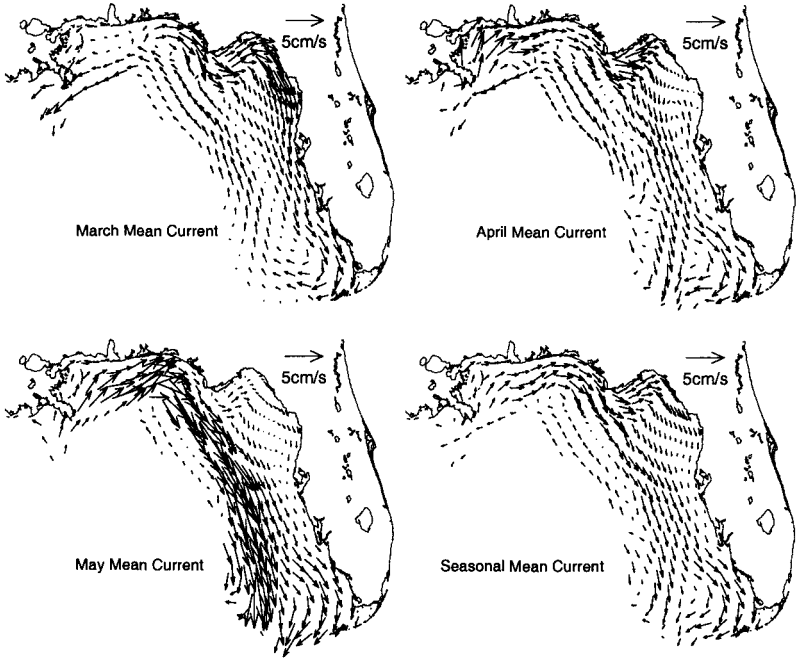

Figure 6 Evolution of the monthly mean, depth averaged velocity vectors for March, April, and May relative to the spring 1999 seasonal mean.

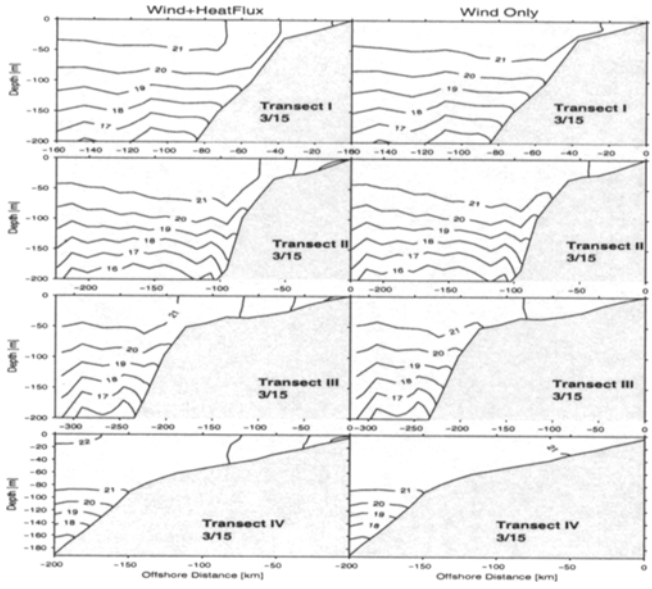

Figure 7 (a) Modeled temperature sections sampled on March 15 across transects originating at DeSoto Canyon, Cape San Blas, Florida Big Bend, and Sarasota. The contour interval is 1°C.

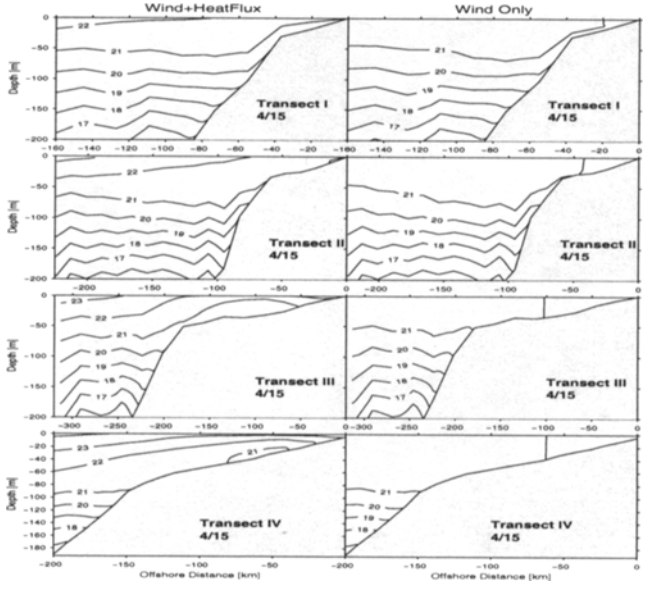

Figure 7 (b) Same as Figure 7(a), except sampled on April 15.

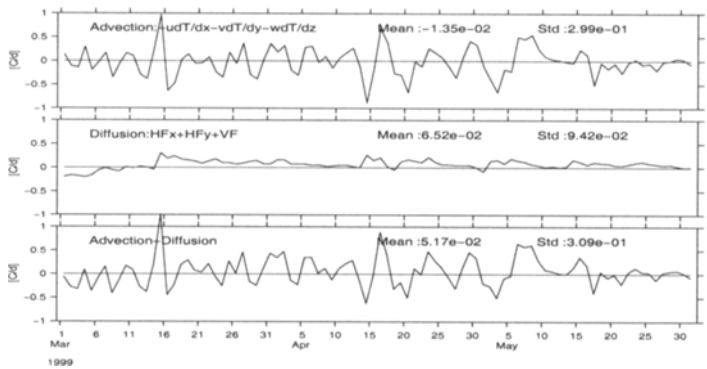

Figure 8 (a) The relative contributions to the depth-averaged temperature balance by ocean circulation and diffusion at station C. Three time series are shown: the advection, the diffusion, and their sum (which equals the local rate of change of depth-averaged temperature). Accompanying each time series are their seasonal means and standard deviations in units of $^{o}C\ day^{-1}$ as measures of the seasonal and synoptic scale variability.

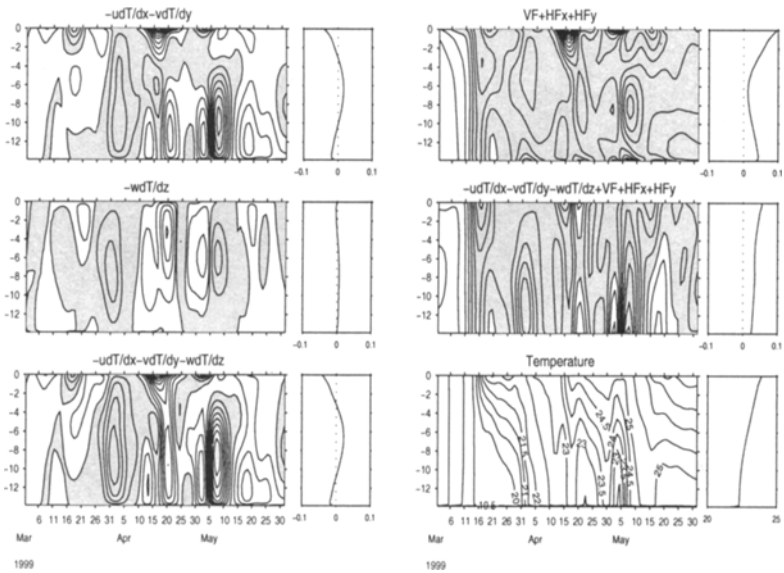

Figure 8 (b) Time series of the depth profiles of the individual terms that comprise the temperature balance at station C. The left hand panels show the horizontal and vertical components of the ocean advection and their sum, and the right hand panels show the diffusion, the diffusion plus the advection, and the temperature. To the right of each panel is the seasonal mean profile. The contour interval for each of the budget terms is $0.05^{o}C\ day^{-1}$, and the contour interval for temperature is $0.5^{o}C$. Shading indicates warming and clear indicates cooling.